

November 2, 2018

## High Amplitude $\delta$ -Scutis in the Large Magellanic Cloud

A. Garg<sup>1,2</sup>, K. H. Cook<sup>1,2</sup>, S. Nikolaev<sup>1</sup>, M. E. Huber<sup>2,3</sup>, A. Rest<sup>4,5,6</sup>, A. C. Becker<sup>7</sup>, P. Challis<sup>2,8</sup>,  
A. Clocchiatti<sup>9</sup>, G. Miknaitis<sup>2,11</sup>, D. Minniti<sup>9,10</sup>, L. Morelli<sup>12</sup>, K. Olsen<sup>5,13</sup>, J. L. Prieto<sup>2,14</sup>, N. B.  
Suntzeff<sup>5,15,16</sup>, D. L. Welch<sup>2,17</sup>, W. M. Wood-Vasey<sup>2,18</sup>

### ABSTRACT

We present 2323 High-Amplitude  $\delta$ -Scuti (HADS) candidates discovered in the Large Magellanic Cloud (LMC) by the SuperMACHO survey (Rest et al. 2005). Frequency analyses of these candidates reveal that several are multimode pulsators, including 119 whose largest amplitude of pulsation is in the fundamental (F) mode and 19 whose

---

<sup>1</sup>Lawrence Livermore National Laboratory, Institute of Geophysics and Planetary Physics, 7000 East Ave., Livermore, CA 94550

<sup>2</sup>Visiting Astronomer, Cerro Tololo Inter-American Observatory, National Optical Astronomy Observatory, which is operated by the Association of Universities for Research in Astronomy, Inc. (AURA) under cooperative agreement with the National Science Foundation

<sup>3</sup>Johns Hopkins University, Baltimore, MD 21218

<sup>4</sup>Dept. of Physics, Harvard University, 17 Oxford Street, Cambridge, MA 02138

<sup>5</sup>Cerro Tololo Inter-American Observatory, National Optical Astronomy Observatory (CTIO/NOAO), Colina el Pino S/N, La Serena, Chile

<sup>6</sup>Goldberg Fellow

<sup>7</sup>Dept. of Astronomy, University of Washington, Box 351580, Seattle, WA 98195

<sup>8</sup>Harvard-Smithsonian Center for Astrophysics, 60 Garden St., Cambridge, MA 02138

<sup>9</sup>Dept. of Astronomy, Pontificia Universidad Católica de Chile, Casilla 306, Santiago 22, Chile

<sup>10</sup>Vatican Observatory, V00120 Vatican City State, Italy

<sup>11</sup>Center for Neighborhood Technology, 2125 W. North Ave., Chicago IL 60647

<sup>12</sup>Dipartimento di Astronomia, Università di Padova, vicolo dell'Osservatorio 3, I-35122 Padova, Italy

<sup>13</sup>National Optical Astronomy Observatory, 950 N. Cherry Ave., Tucson, AZ 85719

<sup>14</sup>Dept. of Astronomy, Ohio State University, 140 West 18th Ave., Columbus, OH 43210

<sup>15</sup>Dept. of Physics and Astronomy, Texas A&M University, College Station, TX 77843-4242

<sup>16</sup>Mitchell Institute for Fundamental Physics, Texas A&M University, College Station, TX 77843-4242

<sup>17</sup>Dept. of Physics and Astronomy, McMaster University, Hamilton, Ontario, L8S 4M1, Canada

<sup>18</sup>Dept. of Physics and Astronomy, University of Pittsburgh, 3951 O'Hara St., Pittsburgh, PA 15260

largest amplitude of pulsation is in the first overtone (FO) mode. Using Fourier decomposition of the HADS light curves, we find that the period-luminosity (PL) relation defined by the FO pulsators does not show a clear separation from the PL-relation defined by the F pulsators. This differs from other instability strip pulsators such as type c RR Lyrae. We also present evidence for a larger amplitude, subluminous population of HADS similar to that observed in Fornax (Poretti et al. 2008).

*Subject headings:* surveys—Magellanic Clouds—*Facilities:* Blanco ()

## 1. Introduction

$\delta$ -Scuti variables populate the region of the Hertzsprung-Russell diagram where the instability strip meets the main sequence. The high-amplitude variables are generally believed to be pulsating primarily in radial modes, whereas  $\delta$ -Scutis with smaller amplitudes are believed to have many non-radial modes of pulsation. Breger (2000) provides a thorough review of the theoretical models describing  $\delta$ -Scuti pulsation. Recent space-based observations from the CoRoT telescope have begun to reveal the rich complexity of  $\delta$ -Scuti pulsation modes (Poretti et al. 2009).

Despite their multimode nature, HADS have been shown to define a period-luminosity relationship, allowing for their use as standard candles (McNamara et al. 2007; Poretti et al. 2008, and references therein). Until recently, observations of large sets of HADS have been limited due to these stars’ intrinsic faintness and short periods. The majority of known HADS have been found within the Milky Way (e.g. Minniti et al. 1998, Alcock et al. 2000a, and Pigulski et al. 2006). More recent work has revealed 90  $\delta$ -Scutis (or SX Phoenicis stars, Population II  $\delta$ -Scutis) in Fornax (Poretti et al. 2008, hereafter P08). Using a subset of the MACHO project data, Lepischak (2007) finds 101  $\delta$ -Scutis in the LMC. McNamara et al. (2007) report 24  $\delta$ -Scutis in the LMC using the OGLE-II data set. Their work also provides a summary of HADS detected by ground-based surveys.

In this paper we present analyses of a large set of  $\delta$ -Scutis discovered by the SuperMACHO survey of the LMC. In Section 2 we provide an overview of the survey and data reduction. In Section 3 we discuss our data and HADS selection criteria, and we present our candidates. We discuss our findings in Section 4. We perform a frequency spectrum analysis of the HADS candidates to identify multimode pulsators and present evidence for a large set of FO pulsators. We examine a subset of our candidates having larger amplitudes. We find evidence for an excess population of faint sources, and discuss whether it is the subluminous population observed in Fornax (P08).

## 2. The SuperMACHO Survey: Observations and Image Reduction

### 2.1. Survey overview

The SuperMACHO project is a five-year optical survey of the Large Magellanic Cloud (LMC) aimed at detecting microlensing of LMC stars (Rest et al. 2005). The goal of this survey is to determine the location of the lens population responsible for the excess microlensing rate observed toward the LMC by the MACHO project (see Alcock et al. 2000b, and references therein) and, thereby, better constrain the fraction of MAssive Compact Halo Objects (MACHOs) in the Galactic halo. The survey was conducted on the CTIO Blanco 4m telescope using a custom *VR* broadband filter with the MOSAIC II wide-field imager. Garg et al. (2007), Miknaitis et al. (2007), Garg (2008a), and Rest & Garg (2008) provide a more complete description of the survey observations and data reduction. Here we provide a brief overview of key elements of the observations and data reduction. During each year of the survey, SuperMACHO observed 68 LMC fields over  $\sim 30$  half-nights during dark and gray time between the months of September – January. The nights and data reduction pipeline were shared with the ESSENCE survey (Miknaitis et al. 2007; Wood-Vasey et al. 2007). The SuperMACHO survey was completed in January 2006.

### 2.2. Object selection

Variable objects are identified using the difference imaging algorithm developed by Alard and Lupton (Alard & Lupton 1998; Alard 2000). The technique is implemented using the “High Order Transform of PSF and Template Subtraction” (HOTPANTS) software package.<sup>1</sup> Excess or negative flux, “difference flux”, detections with a signal-to-noise (S/N)  $> 5$  are matched between images. Those coincident within  $0.54''$  (2 pixels) of each other from image-to-image are assumed to belong to the same source, and the average position of these detections is taken as the source position. If there are at least three detections of a source in any survey year, we identify the source as a “real” variable object.

### 2.3. Difference-image photometry

Once we have identified a source as variable, we perform fixed-centroid, or *forced*, photometry at the detection centroid to obtain a complete difference flux light curve (Garg et al. 2007; Garg 2008a). We measure the difference flux using a modified version of DoPHOT (Schechter et al. 1993) that identifies sources of negative flux. Because there are few actual sources of difference flux and many artifacts in any difference image, we cannot use the difference image itself to determine the point spread function (PSF). Instead we use the PSF determined for the science image prior

---

<sup>1</sup>See online manual at <http://www.astro.washington.edu/becker/hotpants.html>.

to image differencing. We also force the centroid to be at the position determined by the high S/N difference flux detections.

Because we neglect covariance terms when convolving the images for differencing, we find that we underestimate the noise in the difference image. To empirically correct for this, we obtain the flux and its uncertainty for a grid of positions across the difference image using aperture photometry. If the flux uncertainties reflect the Poisson noise, then we would expect a histogram of  $\text{flux}/\delta\text{flux}$  to exhibit a gaussian distribution centered at 0.0 with a standard deviation of 1.0. For a typical image we find the standard deviation to be closer to 1.5, so we adjust our flux uncertainties so that they give a standard deviation of 1.0 which provides a more accurate estimate of the uncertainty in the measured flux (Garg 2008a). We also find that because it uses an analytical PSF model that does not reflect additional structure in the PSF, DoPHOT further underestimates the uncertainty in the measured flux by 0.01 mag (Garg 2008a). We add this term in quadrature to the adjusted uncertainty returned by our modified DoPHOT to obtain the uncertainties reported in this paper.

## 2.4. Multi-band imaging

In addition to the *VR* survey images, we also obtained a set of high quality *B*- and *I*-band images. We process these images using the reduction pipeline described above. We create *B* and *I* catalogs for these images and generate *B* – *I* color-magnitude diagrams (CMD) for each field. Though the MOSAIC II camera does not allow for simultaneous imaging in multiple bands, these observations were typically made within 5 minutes of each other. The colors for even relatively short period variables (1-2 hours) should be sufficiently accurate to determine the rough position of sources in the CMD.

# 3. Data and Results

## 3.1. Initial light-curve phasing

After identifying all variable sources detected by SuperMACHO, we phase their light curves to find periodic variables. We perform light curve phasing using both the SuperSmoother algorithm (Reimann 1994) and the CLEANest code (Foster 1995). For SuperSmoother we use the period that gives the SuperSmoother curve with the smallest residuals. For CLEANest we use the period corresponding to the highest power frequency from the light curve’s frequency spectrum. For the initial candidate selection, we take the shorter of the two periods to be the light curve’s period, *P*. For the objects presented in this paper, this is typically the period determined by CLEANest. For all periodic variables, we find the mean of the difference flux light curve (which may be negative). We add this to the template flux to determine the mean magnitude of the variable object, *VR*.

### 3.2. Candidate selection

We present 2323 light curves of high-amplitude  $\delta$ -Scutis (HADS) in the LMC discovered by the SuperMACHO project. We use the following criteria to select these objects:

1. Using the values of  $P$  and  $VR$  from the initial phasing, we create a period-luminosity (PL) diagram. We find an overdensity of sources that lie roughly in the region expected for  $\delta$ -Scutis in the LMC. Based on the PL diagram, we define this region as  $19.7 < VR < 22.2$  and  $0.045 < P < 0.145$ .
2. We select a higher-amplitude subset of these candidates. We choose only light curves for which the difference between the brightest and faintest data points is greater than 0.2 mag.
3. We cross-match the set of light curves against the  $B$  and  $I$  catalogs described in Section 2.4 using a match radius of  $0.27''$  (1 pixel). We remove candidates that do not have matches in both bands. We also remove candidates that do not lie in the Main-Sequence portion of the CMD. To ensure this, we require each candidate to have  $I > 19.5$  mag and  $0.0 \text{ mag} < B - I < 1.3 \text{ mag}$ . Figure 1 shows the CMD for all SuperMACHO sources falling on a single amplifier and the location of the  $\delta$ -Scuti candidates. After applying these selection criteria, we have 4126 candidate sources.
4. We use the SigSpec (Reegen 2007) code to determine the frequency spectrum of the light curve (see Section 4.2). In many cases, the primary frequency of variation found by SigSpec differs from that found during the initial phasing. We select only light curves having a primary frequency of variation with spectral significance,  $f_{\text{sig}}$ , greater than 5.475, which roughly corresponds to a signal-to-noise ratio of 4 (see Reegen 2007). For the remainder of the analysis, we use the frequency associated with the highest amplitude of variability found by SigSpec such that  $P = 1/f_{\text{SigSpec}}$ . Using the newly determined periods, we select only candidates with  $0.045 \text{ days} < P < 0.115 \text{ days}$ .<sup>2</sup>
5. We perform a fourth order Fourier decomposition of the light curves (see Section 3.4). We use the coefficient of the zero<sup>th</sup> order term,  $a_0$ , as the average stellar magnitude and keep candidates with  $19.8 < a_0 < 22.2$ .
6. We determine an overall amplitude using the model curve described by the fourth order Fourier fit. We define the overall amplitude,  $\Delta$ , as the difference between the minimum and maximum points in the model curve, or the peak-to-trough amplitude. We select only those candidates with a  $\Delta$  greater than 0.2 mag. This yields a final set of 2323 HADS candidates. The majority of the candidates eliminated after applying the CMD criteria are eliminated by this amplitude cut.

---

<sup>2</sup>The shorter upper threshold on the period is based on the apparent region of  $\delta$ -Scuti overdensity in the updated PL diagram.

To determine the efficacy of the above selection criteria, we have inspected the light curves by eye. We estimate that  $<2\%$  are contaminants or poorly phased. To retain objective selection criteria, however, we leave them in the final set. Table 1 gives the position, light-curve characteristics, and color information for all the HADS candidates. Figure 2 shows a selection of candidate light curves.

### 3.3. Comparison with other LMC $\delta$ -Scuti sets

We compare our set of  $\delta$ -Scutis to sets obtained from the OGLE-II (Soszynski et al. 2003) and MACHO surveys (Alcock et al. 2000b). McNamara et al. (2007) analyze a catalog of non-RR Lyrae pulsating variables accompanying the main Soszynski et al. (2003) catalog to find evidence of 24  $\delta$ -Scuti candidates in the LMC. We cross-match the McNamara et al. (2007) catalog against the set of *all* SuperMACHO variables, including those we do not classify as  $\delta$ -Scutis. We find only 1 match within  $2.0''$  of the position reported in McNamara et al. (2007). This object, with OGLE-II designation 050309.65-684327.6, also appears in our candidate set as 7151\_smc8\_15 and lies  $1.54''$  from the OGLE-II position. Lepischak (2007) reports 101 HADS discovered in a subset of the MACHO database. Of these, 99 fall within the FOV observed by SuperMACHO. We note that though these objects fall within the SuperMACHO FOV, several may lie within gaps between amplifiers or close to saturated sources that have been masked. We estimate that these considerations eliminate roughly 5% of our FOV. We cross-match the Lepischak (2007) catalog to the set of SuperMACHO variables and find 37 matches within  $2''$  of the MACHO positions. Of these, 17 appear in our set of  $\delta$ -Scuti candidates. A majority of the eliminated matches are removed based on the third criterion described above which requires candidates to lie on the main-sequence described by the  $B - I$  CMD. We find, however, that without this criterion many of the candidates lie along the red branch and have light curves similar to close eclipsing binaries.

We consider why we find so few matches to these catalogs. Some of the sources identified in these catalogs may not meet the variable object selection criteria described in Section 2.2. We find, however, that a cross-match to the set of Blazhko RR Lyrae identified in MACHO (Alcock et al. 2000c) yields matches within  $2''$  for 62% of the MACHO sources in the SuperMACHO FOV. A more thorough investigation of the SuperMACHO variable source detection efficiency will appear in Garg et al. (2010, in prep); however, the larger match fraction to the MACHO RR Lyrae catalog suggests that low detection efficiency is unlikely to account for the entire discrepancy.

We also examine some of the template images at positions where  $\delta$ -Scutis detected in MACHO were not found in SuperMACHO. We do not see any sources in the templates within several arcseconds of these positions. This suggests that the discrepancy does not result from a failure to classify these objects as variable but rather from a lack of sources at these positions. This may suggest differences between our astrometric solutions, though we emphasize that we do find at least one match within  $2''$  in each catalog. If we allow for a much larger match radius of  $5''$ , we find 44 matches to Lepischak (2007) and 3 to McNamara et al. (2007). Of these matches there are no

new candidates that pass our selection criteria. We note that the apparent brightnesses of LMC  $\delta$ -Scutis are very close to the detection limit for both MACHO and OGLE-II. Misclassification of these faint sources would not be surprising in these catalogs.

In addition to the LMC HADS reported by MACHO and OGLE-II, HADS have been reported by the OGLE-III collaboration (Soszynski et al. 2008; Soszyński 2009). Notably the OGLE-III PL diagram suggests that the HADS have longer periods than those discussed in this work. This will be an important area for further investigation when the final catalog becomes available.

### 3.4. Fourier decomposition

Using the period determined by SigSpec, we perform a fourth order Fourier decomposition of the light curve to obtain the coefficients in the series

$$VR(t) = a_o + \sum_{n=1}^4 a_n \cos\left(\frac{2\pi nt}{P}\right) + b_n \sin\left(\frac{2\pi nt}{P}\right) \quad (1)$$

where  $VR(t)$  is the observed  $VR$  magnitude at time  $t$ ,  $n$  counts each order in the decomposition,  $a_n$  and  $b_n$  are the coefficients of each order determined by the fit, and  $P$  is the period. We find that a fourth order expansion is sufficient to capture the structure of the light curves.

Using the Fourier coefficients we calculate several additional parameters describing the light curves.  $A_n$  is the amplitude of pulsation for each order such that  $A_n^2 = a_n^2 + b_n^2$ .  $r_{ij}$  is the ratio of amplitudes such that  $r_{ij} = A_i/A_j$ .  $\phi_n$  is the phase shift for each order such that  $\phi_n = \text{atan}(b_n/a_n)$ .  $\phi_{ij}$  is given by  $\phi_{ij} = \phi_i - \phi_j$ . These parameters are given in Table 2 for all candidates.

## 4. Discussion

### 4.1. Period-Luminosity diagram

Figure 3 shows the period-luminosity (PL) diagram of the final HADS candidates. We note that the PL relation shows a high degree of scatter. This may indicate subgroups within the sample such as the subluminous group observed by P08. To identify such groups, we create a histogram of the PL-relation-corrected luminosity,  $VR_c$ , of the candidates similar to P08 (Figure 4). We assume the slope of the  $V$ -band PL relation reported by P08 without any transformation or metallicity correction. This gives the relation:

$$VR_{c,-3.65} = 3.65 \log_{10} P + VR \quad (2)$$

Using this equation, we fit for the PL relation for the SuperMACHO  $\delta$ -Scutis. Because of the

possibility of subgroups, we perform the fit using the “ridgeline” of the PL diagram. This assumes that the main population of  $\delta$ -Scutis is the most populous. To find the “ridgeline” we first bin the data by period (0.05 day binsize) and then by  $VR$  (20 bins for each period bin). We then take the densest  $VR$  bin for each period bin as the mode. Figure 5 shows the median and mode magnitudes for each bin. Using the mode as the dependent variable and the inverse square root of the number of candidates in each period bin as the uncertainty, we perform a linear, least-squares fit to the data. This yields the PL relation:

$$VR = -3.65 \log_{10} P + 16.68 \pm 0.11 \text{ mag} \quad (3)$$

We also independently determine the slope of the PL relation using the SuperMACHO  $\delta$ -Scutis. We again perform a fit to the ridgeline, this time leaving the slope as a variable parameter. This fit yields the relation:

$$VR = -3.43 \pm 0.26 \log_{10} P + 16.98 \pm 0.30 \quad (4)$$

Similar to Equation 2, we determine the intercept,  $VR_{c,-3.43}$ , for all candidates using the slope from the best fit. Figure 4 shows the histogram of  $VR_{c,-3.43}$  (hereafter,  $VR_c$  refers to the PL-corrected-luminosity using this best fit slope). We examine the impact of our binsize on the best fit to the ridgeline. We find that both doubling and halving the binsize give shallower slopes. In both instances, however, this is because the selected binsize gives too much weight to the sparse region of the PL-diagram at short periods.

## 4.2. Multimode pulsators

In addition to the primary frequency of variation, SigSpec finds lower amplitude modes of variation. We use the SigSpec frequency spectrum to determine whether the candidates show multiple modes of pulsation. We consider any frequency within  $\frac{1}{10}$  of a whole number ratio to the primary frequency to be an alias. We only consider secondary frequencies with a spectral significance greater than 5 (see Reegen 2007). SigSpec does return additional modes with significance greater than 5 for a few candidates. Given the typical signal-to-noise ratio and sampling of the SuperMACHO data, however, we do not consider these to be reliable.<sup>3</sup> Figure 6 shows the ratio between the

---

<sup>3</sup>As described in Section 2.3 Garg (2008a) finds that the typical systematic error in SuperMACHO difference flux measurements is 0.01 mag, and characteristic uncertainties for faint sources are a few percent. The median pulsation amplitude of the  $\delta$ -Scutis is approximately 0.3 mag (see Figure 10), suggesting that typical measurement uncertainties for the faintest sources may be up to 10% of the pulsation amplitude. We also lack sufficient coverage to adequately characterize the properties of many higher frequencies. For example, Poretti et al. (2009) have 140,016 datapoints, while our typical light curve has  $\sim 130$ . Because of the limited coverage and relatively large errors in the light curves, we opt for a conservative cut-off at secondary modes in our multimode analysis.

primary and secondary frequency,  $f_{\text{primary}}/f_{\text{secondary}}$ , as a function of the spectral significance of the secondary. Table 2 gives  $f_{\text{primary}}/f_{\text{secondary}}$  for candidates showing a secondary frequency.

Examination of Figure 6 reveals two distinct groups with high values of  $f_{\text{sig}}$ . We find 119 candidates in the first group with  $0.765 < f_{\text{primary}}/f_{\text{secondary}} < 0.790$ , and we find 19 candidates in the second group with  $1.275 < f_{\text{primary}}/f_{\text{secondary}} < 1.305$  (Figure 7 shows a representative selection of light curves for both groups). The frequency ratios indicate that these groups are multimode fundamental (F) and first overtone (FO) pulsators respectively (see McNamara et al. 2007; Poretti et al. 2005, and references therein). We note that there are several other light curves with  $f_{\text{sig,secondary}}$  greater than 5.0. Inspection of their light curves reveals that while they do show additional scatter, it is not as pronounced as that of the candidates falling into the groups described above (Figure 8 shows a representative selection of these light curves). This may contribute to greater uncertainty in determining the secondary frequency.

Figure 9 shows the Petersen diagram for the multimode F and FO candidates. We have assumed that the candidates with frequency ratios greater than one are varying in overtone modes, and set  $P_0$  as their secondary period. We note that we observe several candidates with ratios above 0.778 whereas Poretti et al. (2005) observe only one. Based on their findings, this is likely an indication that these candidates are metal-poor compared to the Galactic sample. Such an interpretation is consistent with observational measurements of LMC metallicity (Cole et al. 2005).

We note that the multimode pulsators are concentrated toward fainter values of  $VR_c$ . We examine whether the lack of multimode pulsators at the brightest values of  $VR_c$  may be attributable to lower sensitivity to secondary periods for these candidates. A plot of  $\Delta$  against  $VR_c$  (Figure 10) reveals that the brighter sources generally have smaller amplitudes. To determine our ability to detect secondary modes of pulsation, we simulate several double-mode sinusoidal light curves as they would appear in our data (see Garg 2008a,b, and Garg et al. 2010, in prep.). We model the light curves using:

$$VR(t) = A_0 + A_1 \sin(tf_1) + A_1 A_{\text{ratio}} \sin(tf_{\text{ratio}} f_1) \quad (5)$$

where  $VR(t)$  is the  $VR$  magnitude at time  $t$ ,  $A_0$  is the mean magnitude,  $A_1$  is the amplitude of the primary frequency,  $A_{\text{ratio}}$  is the ratio between the amplitude for the primary and secondary frequencies,  $f_1$  is the primary frequency, and  $f_{\text{ratio}}$  is the ratio between the primary and secondary frequency. All parameters except  $f_{\text{ratio}}$  are randomly selected from a uniform distribution. We choose  $A_0$  to be between 19 and 22.5. We choose  $A_1$  between 0.07 and 1.1. We choose  $A_{\text{ratio}}$  between 0.1 and 1.0. We restrict  $f_{\text{ratio}}$  to be either 0.777 or 1.288, corresponding to the ratios for multimode F and FO pulsators respectively. We note that using our definition,  $\Delta$  is equal to twice  $A_1$  in these simulations. We find that our ability to detect secondary modes does not depend strongly on  $A_{\text{ratio}}$ . For values of  $A_{\text{ratio}}$  close to 1.0, we do occasionally misidentify the secondary period as the primary, but overall our detection efficiency is roughly 65–80% for all values of  $A_{\text{ratio}}$  integrated over  $\Delta$ . Using the values of  $A_0$  and  $f_1$ , we determine  $VR_c$  for each simulated light curve

by Equation 4. We also find no strong correlation between  $VR_c$  and our efficiency for detecting secondary modes, though the fainter light curves tend toward the low end of the efficiency range. We do find that our efficiency for detecting secondary modes depends on the amplitude of the primary mode of pulsation,  $A_1$ . For  $A_1$  close to 0.1, corresponding to  $\Delta$  close to 0.2, our detection efficiency for multimodes in FO pulsators ranges from 15–50%. For multimode F pulsators, it is higher and ranges from 40–60%. For no other parameter do the detection efficiencies differ so greatly between F and FO frequency ratios.

### 4.3. Overtone pulsators

The histograms shown in Figure 4 are heavily skewed toward brighter magnitudes. Typically, such a population that lies above the main PL-relation is thought to be pulsating at the overtone frequency (see P08 and references therein). We also find that the multimode FO pulsators identified in Section 4.2 are brighter than the multimode F pulsators, though there is no evidence of secondary pulsation modes in the brightest candidates to help confirm the FO interpretation. As discussed above, we have a low efficiency for detecting multimode overtone pulsators at small amplitudes. We note that Figure 10 indicates that the brightest values of  $VR_c$  correspond to the lowest amplitude candidates. Based on observations and models of RR Lyrae, small amplitudes are consistent with the overtone hypothesis (Bono et al. 1996). As discussed in Section 4.2, small amplitudes also reduce our ability to detect multiple modes particularly in FO pulsators. While the presence of multimode FO pulsators amongst the brightest candidates would lend additional support to the overtone hypothesis, their lack does not rule out this interpretation.

We also examine the shape of the phased light curves using the Fourier components. Based on observations of FO RR Lyrae, we would expect overtone pulsators to exhibit a more symmetric light curve (Stellingwerf et al. 1987; McNamara 2000). By examining the relation between  $r_{21}$  and  $VR_c$  (Figure 11), we find this to be the case. Because  $\phi_{21}$  is relatively constant for all candidates (Figure 12),  $r_{21}$  measures the relative contributions of the second and first fourier components to the overall amplitude. More asymmetric light curves should have higher values of  $r_{21}$ , and we find that lower values of  $VR_c$  correspond to lower values of  $r_{21}$ . This is suggestive that the brighter sources with lower values of  $r_{21}$  may be overtone pulsators having more symmetric light curves.

We plot the difference between the phase of minimum and maximum,  $\phi_{\text{diff}}$ , against  $VR_c$  (Figure 13). For a purely symmetric, sinusoidal light curve, we would expect  $\phi_{\text{diff}}$  to be 0.5. We find that the majority of our candidates lie between 0.35 and 0.4. Notably, however, the FO multimode candidates have larger values of  $\phi_{\text{diff}}$  corresponding to a more symmetric light curve as we would expect. We find, however, no strong correlation between  $\phi_{\text{diff}}$  and  $VR_c$ .

By examining the amplitude and shape of the brightest candidates and comparing to trends observed in RR Lyrae, these light-curve analyses indicate that we may have several candidates pulsating in the first overtone mode. Notably Bono et al. (1997) conclude that the effect may be

reversed for  $\delta$ -Scutis: overtone  $\delta$ -Scutis may exhibit larger amplitudes and more asymmetric light curves. Our data disagree with this finding, however, as the small amplitude candidates examined in this section lie *above* the main PL-relation, indicating that they have shorter periods than the majority of the candidates with similar luminosities.

We also note that unlike FO RR Lyrae and FO Cepheids, we see no clear separation between the F and possible FO  $\delta$ -Scutis. Our results are similar to those of P08 whose PL-diagram also does not show a clear separation. We consider whether the lack of separation indicates significant scatter in the metallicities of the candidates. Such scatter would shift the intercept of the PL-relation and potentially smear the separation between fundamental and overtone pulsators. Cole et al. (2005) do find a significant spread in LMC metallicity based on spectroscopic observations of the Calcium II triplet in red giants toward the bar region. They find a primary population with  $[\text{Fe}/\text{H}] = -0.37$  and  $\sigma = 0.15$  and a second, metal-poor population with  $[\text{Fe}/\text{H}] = -1.08$  and  $\sigma = 0.46$ . Using the metallicity dependence of 0.19  $[\text{Fe}/\text{H}]$  from McNamara et al. (2004), we might expect an additional 0.03 mag of scatter in the PL-relation based on these results.

Differing extinction may also contribute additional scatter. If we assume the reddening distribution is  $E(B - V) = 0.13$  with  $\sigma = 0.045$  (Harris et al. 1997) and  $R_v = 3.1$ , we expect an additional 0.14 mag of scatter from variations in extinction. The tilt of the LMC will also contribute additional scatter of  $\sim 0.01$  mag (Sebo et al. 2002). We examine the uncertainty in our period determinations as this may also contribute to additional scatter. Using the technique used for the multimode light-curve simulations described in Section 4.2, we simulate  $\delta$ -Scuti light curves as they appear in our data. We use the fourier coefficients from our candidate  $\delta$ -Scutis and Equation 1 to model the light curves. We find that the periods we measure for more than 80% of the simulations we recover are within 0.001 days of the input period. The additional scatter contributed from this uncertainty is negligible.

We add in quadrature the additional scatter contributed to  $VR_c$  by the above factors to obtain an expected scatter of 0.14 mag. Inspection of Figure 4, however, reveals that the difference between the mode of  $VR_{c,-3.43}$ , 17.0 mag, and the next-densest bright bin, 16.7 mag, is 0.3 mag. This difference is more than 2 times the additional scatter, large enough that it is difficult to explain the lack of a clear separation between F and FO pulsators based on these factors alone. These data may indicate that a clear separation between the PL-relation for F and FO modes does not exist for  $\delta$ -Scutis. This is not necessarily surprising.  $\delta$ -Scutis lie in a region of the instability strip that spans a wide range of temperatures and luminosities. Because of this we would expect the PL-diagram to have a broad intrinsic width resulting in regions of FO pulsation that overlap regions of F pulsation.

#### 4.4. Larger amplitude population

The histogram of  $VR_c$  shows no strong indication of the subluminal population described in P08. We find, however, that the median  $\Delta$  increases for fainter sources (Figure 10). To test whether this reflects a selection bias against smaller amplitudes for fainter sources, we use the simulations of  $\delta$ -Scuti light curves described in Section 4.3. We find that while we have a relatively high efficiency for detecting  $\delta$ -Scutis at all amplitudes and luminosities considered ( $>65\%$ ), for the faintest sources we are  $\sim 13\%$  more efficient at detecting larger amplitude ( $0.8 \text{ mag} < \Delta < 1.0 \text{ mag}$ ) variables than smaller amplitude ( $0.2 \text{ mag} < \Delta < 0.4 \text{ mag}$ ) variables. The ratio between detection efficiencies for different amplitudes is similar for brighter sources. Figure 14 shows the median and 33<sup>rd</sup> percentile error bars after correcting for detection efficiency. We find that the median amplitude still increases with  $VR_c$ .

We also find that the majority of sources with  $\Delta > 0.4 \text{ mag}$  have  $VR_c$  fainter than 16.8 mag. We note that the sources in P08 also have larger amplitudes, generally greater than 0.4 mag. A histogram of only the SuperMACHO LMC candidates with  $\Delta > 0.4 \text{ mag}$  also indicates an excess of subluminal sources similar to that observed by P08 (Figure 15). We suggest that the subluminal population described in P08 may reflect these larger amplitude sources.

As discussed in P08, the explanation for these sources remains an open question. Observations and models of RR Lyrae show that for fundamental pulsators amplitude increases at lower metallicities (Bono et al. 1996). This may suggest that these candidates represent a more metal-poor population. We consider whether they may belong to the metal-poor LMC population observed by Cole et al. (2005) having  $[\text{Fe}/\text{H}] = -1.08 \pm 0.46$ . Again using the metallicity dependence from McNamara et al. (2004) of 0.19  $[\text{Fe}/\text{H}]$ , we would expect  $\delta$ -Scutis from this population to lie 0.21 mag below the main PL-relation. Our data show a larger separation of almost 0.4 mag. Notably, the separation between the main and subluminal populations observed by P08 is similar. Given the differences in the compositions and star-formation histories of Fornax and LMC, this similarity lends support to the conclusion that these large amplitude, subluminal sources evolved from the same population as those on the main PL-relation. It would otherwise be difficult to explain why both galaxies have such similar larger amplitude, subluminal populations that evolved independently.

## 5. Conclusion

We have discovered 2323 candidate HADS in the Large Magellanic Cloud (LMC) using the SuperMACHO set of variables. Using the SigSpec software, we performed frequency analyses of these candidates which reveal several multimode pulsators, including 119 that are pulsating fundamental modes and 19 in first overtone modes. We find evidence for a large set of FO pulsators within this data set. Notably, the PL-relation defined by the FO pulsators does not show a clear separation from the PL-relation defined by the F pulsators. This is not necessarily surprising, as

$\delta$ -Scutis occupy a region of the instability strip that spans a broad region of temperatures, and hence intrinsic color. Though we are unable to do so with our single-epoch multi-band photometry, future surveys that obtain multi-epoch color information may be able to better define this region of the CMD. Such data would also allow for the determination of period-luminosity-color (PLC) corrected magnitudes that would reveal whether a clear separation between F and FO pulsators does exist.

We also find that the majority of our HADS with amplitudes greater than 0.4 mag lie below the ridgeline of the PL-diagram. By examining only these candidates, we find an excess of subluminoous sources similar to that observed in Fornax (P08). Because the separation between this population and the main PL-relation is also similar to that found in Fornax, despite its having different composition and formation history, we postulate that they form at the same time as those on the main PL-relation rather than constituting a second, older and metal-poor population. Spectroscopic observations to measure the metallicities of these stars may help to illuminate this discussion.

## 6. Acknowledgments

We would like to thank D. H. McNamara for his helpful insights into this data set. The SuperMACHO survey was undertaken under the auspices of the NOAO Survey Program. We are very grateful for the support provided to the Survey program from the NOAO and the National Science Foundation. We are particularly indebted to the scientists and staff at the Cerro Tololo Inter-American Observatory for their assistance in helping us carry out the survey. SuperMACHO is supported by the STScI grant GO-10583. We are grateful to members of the ESSENCE supernova survey with whom we work closely. We would also like to thank the High Performance Technical Computing staff at Harvard. AG's, KHC's, MEH's, and SN's work was performed under the auspices of the U.S. Department of Energy by Lawrence Livermore National Laboratory under Contract DE-AC52-07NA27344. C. Stubbs thanks the the McDonnell Foundation for its support through a Centennial Fellowship. C. Stubbs, AG, and AR are also grateful for support from Harvard University. AC acknowledges the support of grant P06-045-F ICM-MIDEPLAN. DM and AC are supported by grants FONDAP CFA 15010003 and Basal CATA 0609. LM is supported by grant (CPDR061795/06) from Padova University. DLW acknowledges financial support in the form of a Discovery Grant from the Natural Sciences and Engineering Research Council of Canada (NSERC).

Table 1.  $\delta$ -Scuti candidates

ID	RA (J2000)	Dec	<i>Period</i> (days)	$\Delta$ (mag)	<i>VR</i>	<i>I</i>	<i>B – I</i>	$N_{obs,VR}$	$f_p/f_s$	Type
2291_sm43_10	06:01:06.66	-72:02:49.8	0.10064	0.33	20.20	19.92	0.99	92	-	-
7345_sm43_10	05:58:57.54	-72:02:40.0	0.05715	0.44	21.32	21.01	0.49	92	-	-
2349_sm44_10	05:59:40.46	-71:27:14.3	0.05988	0.27	21.12	20.74	0.65	86	-	-
6074_sm44_10	05:57:58.41	-71:26:43.9	0.05923	0.45	21.24	20.67	0.50	86	-	-
4223_sm45_10	05:57:47.82	-70:52:19.3	0.07532	0.29	21.08	20.87	1.04	82	-	-
4927_sm45_10	05:57:22.56	-70:51:14.5	0.05847	0.24	21.32	21.09	0.97	82	-	-
3263_sm46_10	05:57:46.09	-70:15:27.2	0.06759	0.54	20.40	20.24	0.80	90	-	-
11884_sm46_10	05:55:20.03	-70:14:45.3	0.05115	0.55	20.76	20.26	0.73	90	-	-
7207_sm53_10	05:51:39.46	-72:04:59.6	0.05647	0.38	21.38	21.00	0.42	95	-	-
12190_sm54_10	05:50:15.01	-71:25:50.2	0.08754	0.30	20.27	20.06	0.50	83	-	-
18598_sm55_10	05:50:05.53	-70:52:23.0	0.06846	0.22	20.93	20.50	0.64	80	1.400	double
16664_sm56_10	05:48:30.61	-70:16:43.6	0.08034	0.24	20.52	20.26	0.80	75	-	-
10335_sm57_10	05:48:40.49	-69:40:49.5	0.06836	0.37	20.68	20.39	0.98	92	-	-
12731_sm58_10	05:47:53.57	-69:02:16.2	0.05311	0.43	21.47	21.14	0.87	69	-	-
14258_sm58_10	05:47:40.23	-69:03:21.2	0.07120	0.27	20.66	20.52	1.09	69	-	-
1859_sm63_10	05:46:07.28	-72:02:02.5	0.06176	0.33	21.03	20.56	0.74	90	-	-
2644_sm64_10	05:45:32.38	-71:29:03.6	0.04764	0.36	21.34	20.98	0.82	76	-	-
6269_sm64_10	05:44:44.15	-71:27:29.0	0.08055	0.36	20.47	20.22	0.76	78	-	-
1783_sm66_10	05:44:34.91	-70:15:12.8	0.11447	0.28	20.57	20.21	1.01	88	-	-
14300_sm66_10	05:43:01.99	-70:13:31.5	0.08786	0.22	20.19	19.83	0.90	52	-	-
18683_sm66_10	05:42:33.14	-70:16:36.4	0.07284	0.41	20.61	20.29	0.94	88	-	-

Note. — *ID* is the object label for each candidate. *Period* is the primary period of pulsation in days.  $\Delta$  is the overall, peak-to-trough amplitude of *VR*-band variation in magnitudes.  $N_{obs,VR}$  gives the number of *VR*-band observations.  $f_p/f_s$  is the primary frequency of variation over the secondary frequency of variation. *Type* indicates whether the candidate shows multiple modes of pulsation. *F* and *FO* refer to objects identified through their secondary frequencies as double-mode fundamental and first overtone pulsators respectively.

Table 2.  $\delta$ -Scuti Fourier Parameters

ID	<i>Period</i> (days)	$\Delta$ (mag)	<i>VR</i>	<i>I</i>	<i>B</i> − <i>I</i>	<i>A</i> <sub>1</sub>	<i>A</i> <sub>2</sub>	<i>A</i> <sub>3</sub>	<i>A</i> <sub>4</sub>	<i>r</i> <sub>21</sub>	<i>r</i> <sub>31</sub>	<i>r</i> <sub>41</sub>	$\phi_{21}$	$\phi_{31}$	$\phi_{41}$	$\phi_{diff}$
2291_sm43_10	0.10064	0.33	20.20	19.92	0.99	0.14	0.04	0.01	0.00	0.29	0.10	0.03	2.53	6.22	1.93	0.42
7345_sm43_10	0.05715	0.44	21.32	21.01	0.49	0.20	0.05	0.02	0.01	0.26	0.10	0.03	2.53	5.45	1.16	0.43
2349_sm44_10	0.05988	0.27	21.12	20.74	0.65	0.12	0.04	0.02	0.00	0.36	0.13	0.01	2.53	5.55	0.99	0.43
6074_sm44_10	0.05923	0.45	21.24	20.67	0.50	0.18	0.06	0.02	0.02	0.32	0.09	0.10	2.33	5.72	1.95	0.39
4223_sm45_10	0.07532	0.29	21.08	20.87	1.04	0.12	0.05	0.02	0.01	0.43	0.17	0.11	2.45	4.93	1.39	0.37
4927_sm45_10	0.05847	0.24	21.32	21.09	0.97	0.11	0.03	0.01	0.00	0.23	0.10	0.02	2.77	5.60	2.55	0.47
3263_sm46_10	0.06759	0.54	20.40	20.24	0.80	0.23	0.07	0.01	0.02	0.33	0.06	0.07	2.40	4.83	2.20	0.36
11884_sm46_10	0.05115	0.55	20.76	20.26	0.73	0.25	0.09	0.03	0.01	0.36	0.13	0.04	2.51	4.90	0.85	0.36
7207_sm53_10	0.05647	0.38	21.38	21.00	0.42	0.17	0.05	0.03	0.01	0.28	0.16	0.04	2.69	5.14	2.68	0.52
12190_sm54_10	0.08754	0.30	20.27	20.06	0.50	0.13	0.05	0.01	0.01	0.39	0.06	0.05	2.37	3.99	4.06	0.33
18598_sm55_10	0.06846	0.22	20.93	20.50	0.64	0.09	0.02	0.02	0.01	0.20	0.19	0.15	2.90	6.06	3.00	0.43
16664_sm56_10	0.08034	0.24	20.52	20.26	0.80	0.11	0.03	0.00	0.00	0.28	0.03	0.03	2.37	5.06	5.20	0.38
10335_sm57_10	0.06836	0.37	20.68	20.39	0.98	0.15	0.04	0.02	0.02	0.27	0.15	0.14	2.53	6.08	2.31	0.41
12731_sm58_10	0.05311	0.43	21.47	21.14	0.87	0.18	0.05	0.02	0.02	0.28	0.11	0.10	2.53	5.30	1.76	0.40
14258_sm58_10	0.07120	0.27	20.66	20.52	1.09	0.12	0.03	0.01	0.01	0.23	0.07	0.10	2.47	5.63	1.74	0.40
1859_sm63_10	0.06176	0.33	21.03	20.56	0.74	0.15	0.04	0.01	0.00	0.30	0.04	0.03	2.56	5.98	2.15	0.39
2644_sm64_10	0.04764	0.36	21.34	20.98	0.82	0.15	0.06	0.01	0.01	0.43	0.04	0.08	2.49	1.06	1.84	0.37
6269_sm64_10	0.08055	0.36	20.47	20.22	0.76	0.14	0.06	0.01	0.02	0.41	0.10	0.11	2.21	2.97	2.82	0.34
1783_sm66_10	0.11447	0.28	20.57	20.21	1.01	0.12	0.04	0.01	0.01	0.29	0.09	0.07	2.07	4.56	1.48	0.37
14300_sm66_10	0.08786	0.22	20.19	19.83	0.90	0.10	0.03	0.01	0.01	0.29	0.06	0.06	2.17	2.90	3.85	0.36
18683_sm66_10	0.07284	0.41	20.61	20.29	0.94	0.18	0.04	0.02	0.01	0.22	0.13	0.06	2.67	0.09	1.01	0.45

Note. — *ID* is the object label for each candidate. *Period* is the primary period of pulsation in days.  $\Delta$  is the overall, peak-to-trough amplitude of *VR*-band variation in magnitudes.  $A_n$ ,  $r_{n1}$ ,  $\phi_{n1}$   $\phi_{diff}$  are parameters describing the light curves based on a Fourier decomposition (Section 3.4).

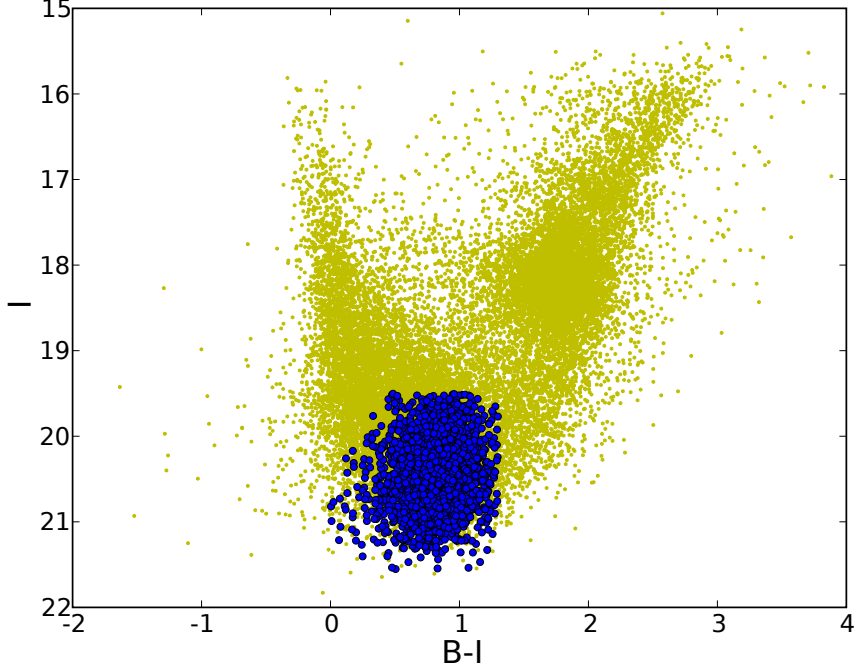


Fig. 1.—  $B - I$  color-magnitude diagram. Yellow dots show all star-type sources in the  $B$  and  $I$  catalog for a single amplifier in field sm97. The CMD is similar for all SuperMACHO fields. The filled blue circles show the final set of HADS candidates. Candidate selection criteria include the requirement that the source lie on the main-sequence.

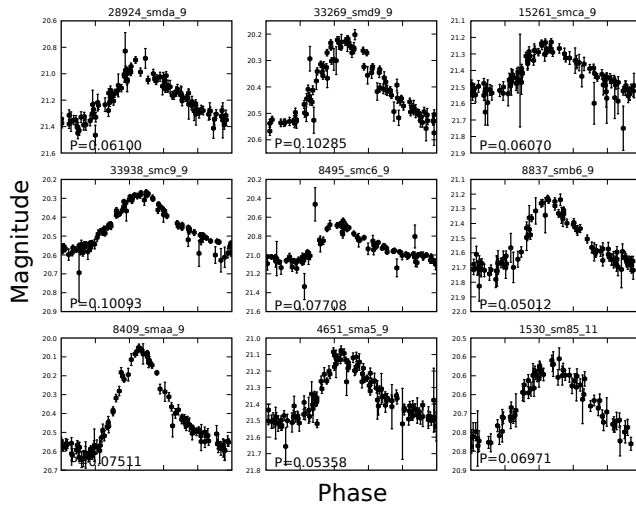


Fig. 2.— Light curves for a selection of  $\delta$ -Scuti candidates.

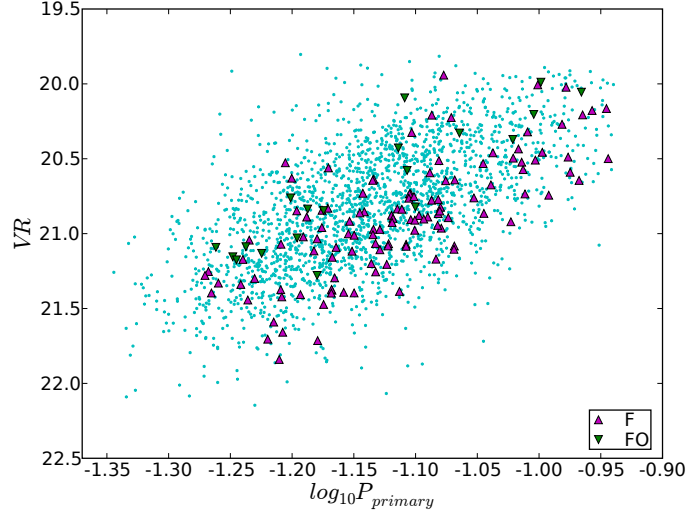


Fig. 3.— Period-Luminosity diagram. The cyan dots show all  $\delta$ -Scuti candidates. The green pentagons show multimode FO pulsators, and the maroon diamonds show multimode F pulsators (see Section 4.2).

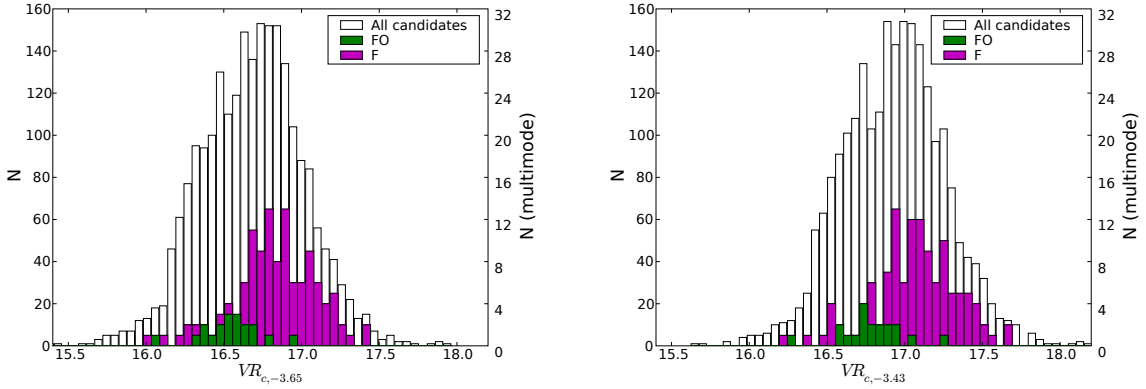


Fig. 4.— Figure showing the histogram of PL-relation-corrected luminosities,  $VR_c$ . We show histograms for the PL-relation-corrected magnitudes of the candidates using both the slope from P08 (left) and the slope independently determined from this data (right). The double-mode F and FO pulsators are overplotted in maroon and green respectively. The histograms of the double-mode candidates are scaled for visibility, and the scaling is shown on the right y-axis. For both slopes, we find the histogram is skewed toward brighter sources. This excess of brighter sources is often interpreted as evidence of overtone mode pulsators (see Section 4.3).

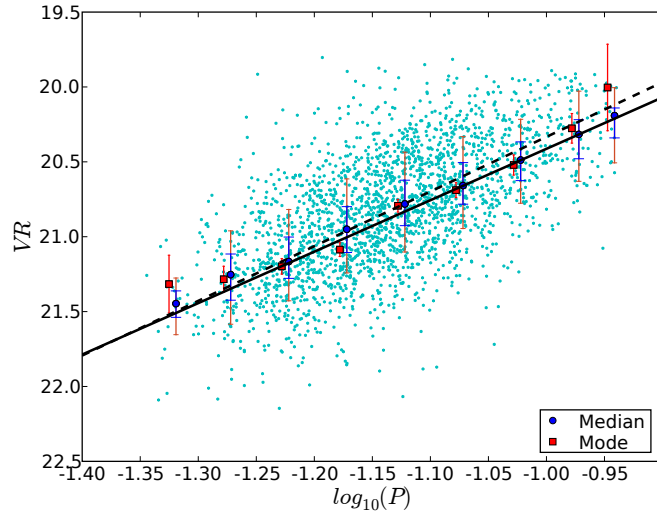


Fig. 5.— PL-diagram of all candidates with fitted PL-relation. The cyan dots show all  $\delta$ -Scuti candidates. The blue circles give the median magnitudes for each period. The blue and orange error bars show the 33<sup>rd</sup> and 66<sup>th</sup> percentiles of the population respectively, i.e. 33% ( $\pm 17.5\%$ ) and 66% ( $\pm 33\%$ ) of the candidates within each bin lie between the ends of the error bars. We note that the distribution in each bin is not always symmetric about the median. The red squares show the mode for each bin, and their errors show the inverse square root of the number of sources in the bin. To improve visibility, we show the median and mode values slightly offset from the center of the bin position. The solid line is the best fit PL relation to the modes (see Equation 4). The dashed black line is the best fit PL relation when fixing the slope to that given by P08 (see Equation 3).

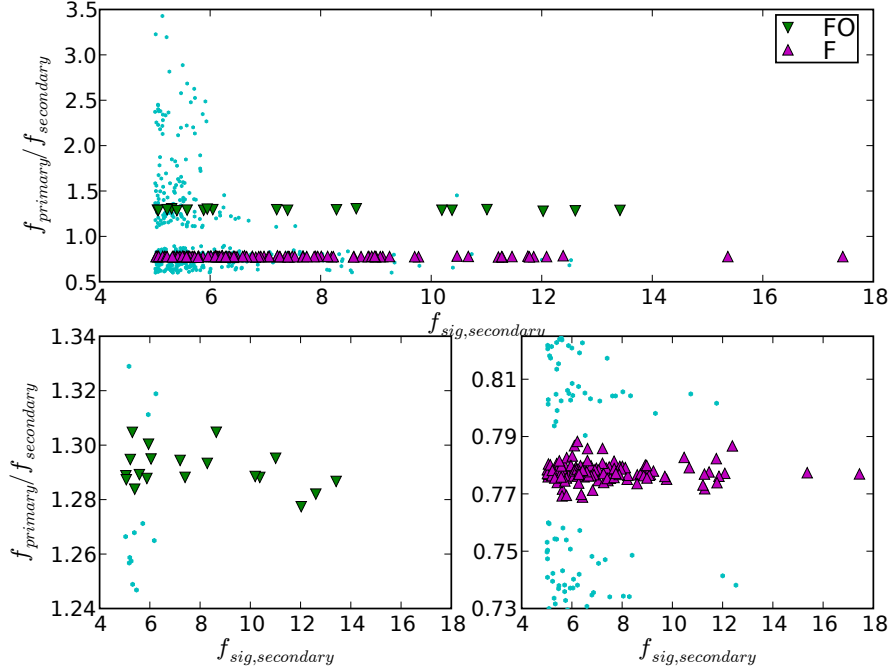


Fig. 6.— Ratio between primary and secondary frequencies against  $f_{\text{sig,secondary}}$ . We plot the ratio of the primary to the secondary frequency of variability against the significance of the secondary frequency for all candidates showing secondary frequencies with significance greater than 5 (see Reegen 2007). We have removed any candidates showing only secondary frequencies that have whole number ratios to the primary. We find 119 candidates with  $0.765 < f_{\text{primary}}/f_{\text{secondary}} < 0.790$  (green pentagons) and 19 candidates with  $1.275 < f_{\text{primary}}/f_{\text{secondary}} < 1.305$  (maroon diamonds). These likely correspond to double-mode and overtone pulsators respectively. We note the appearance of less dense additional clusters of candidates with secondary modes at frequency ratios of  $\sim 0.74$  and  $\sim 0.8$ , and we identify an outlier at  $f_{\text{primary}}/f_{\text{secondary}} = 1.452$ . The close proximity to of these clusters to ratios with the first overtone frequency suggest that these may also belong to the groups described above. As shown in Figure 8, these light curves show significantly less scatter with respect to their characteristic photometric uncertainties than those falling into the above classifications, even for similar values of  $f_{\text{sig,secondary}}$ . We conclude that the secondary frequency determination for these sources may be unreliable.

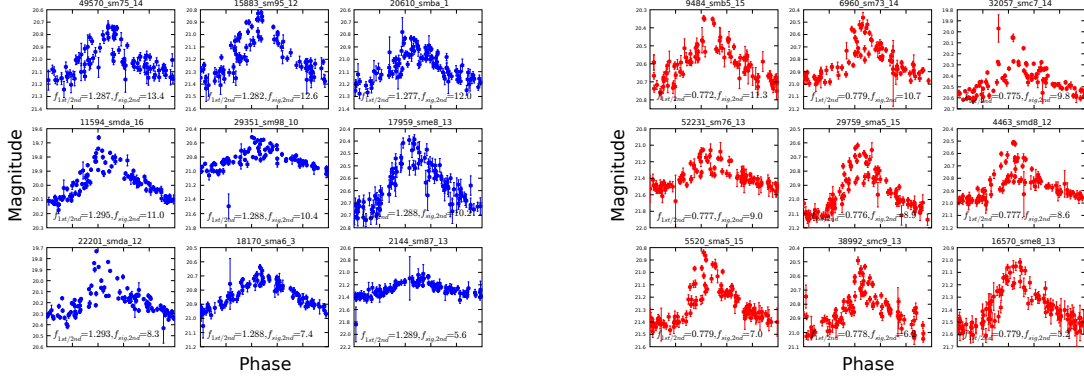


Fig. 7.— Light curves for a selection of candidates showing secondary periods with  $f_{\text{sig}} > 5.0$ . The plot on the left shows candidates with  $1.275 < f_{\text{primary}}/f_{\text{secondary}} < 1.305$ . The plot on the right shows candidates with  $0.765 < f_{\text{primary}}/f_{\text{secondary}} < 0.790$ . These groups correspond to multimode first overtone and fundamental pulsators respectively.

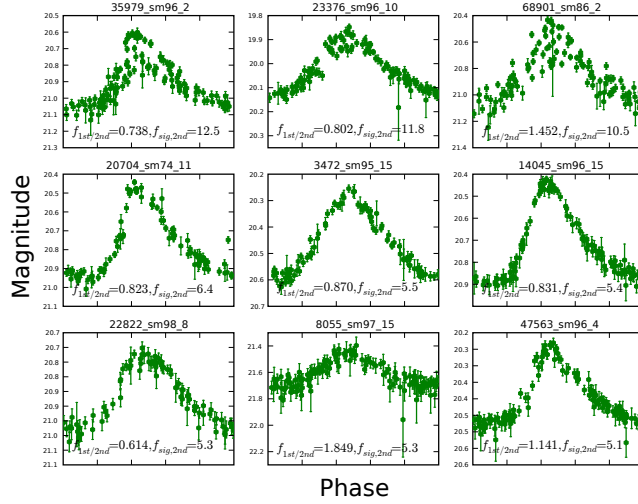


Fig. 8.— Light curves for a selection of candidates showing secondary periods with  $f_{\text{sig}} > 5.0$ . The ratio  $f_{\text{primary}}/f_{\text{secondary}}$  does not fall into the range for either F or FO pulsators. These candidates also show somewhat less scatter with respect to their characteristic photometric uncertainties. This suggests that the pulsation amplitudes for both modes may be similar which may contribute error to the secondary frequency determination.

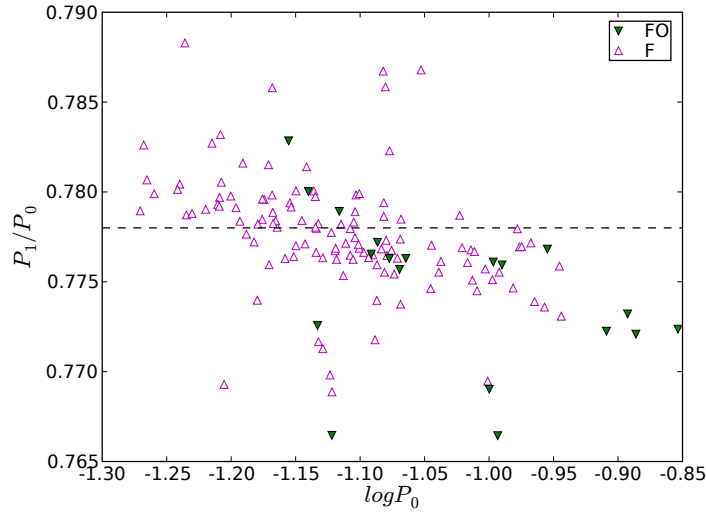


Fig. 9.— Petersen diagram. We show the Petersen diagram for multimode F (open maroon diamonds) and FO (green pentagons) candidates. We find several candidates with  $P_1/P_0$  greater than 0.778 (shown as a dashed line). These values are higher than those observed by Poretti et al. (2005). Higher ratios may be indicative of lower metallicity stars. Suárez et al. (2006) also find that higher rotational velocities can yield higher ratios; however, their work suggests that the impact of rotation is reduced at lower metallicities and shorter periods.

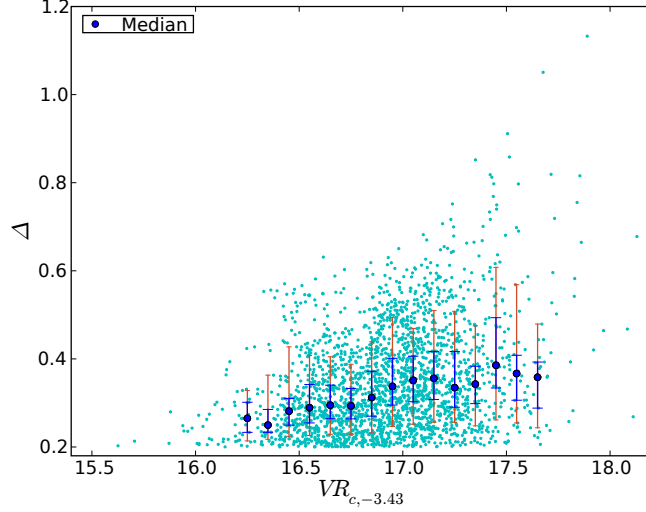


Fig. 10.—  $\Delta$  against  $VR_c$  for all candidates.  $\Delta$  gives the peak-to-trough amplitude of the phased light curve. We bin the candidates by  $VR_c$ . The blue circles show the median amplitudes for each bin. The error bars show the 33<sup>rd</sup> and 66<sup>th</sup> percentile as described in the caption of Figure 5. We do not show bins containing fewer than 20 candidates. We find that the brightest candidates have the lowest amplitudes. We also find few candidates having  $\Delta > 0.4$  mag that are brighter than  $VR_c = 16.8$ .

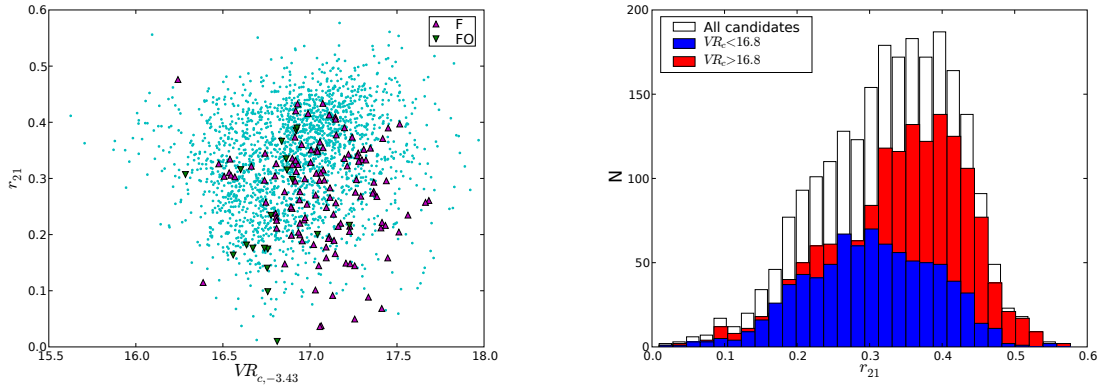


Fig. 11.—  $r_{21}$  against  $VR_c$  and histogram of  $r_{21}$  for all candidates. Because  $\phi_{21}$  is similar for all candidates (see Figure 12),  $r_{21}$  measures the relative contributions of the second and first fourier components to the overall amplitude. See caption of Figure 3 for description symbols in the left panel. In the right panel, white bars show the histogram of  $r_{21}$  for all candidates. Overplotted in red are fainter candidates with  $VR_c > 16.8$ . Overplotted in blue are brighter candidates with  $VR_c < 16.8$ . We find that the brighter values of  $VR_c$  also have smaller values of  $r_{21}$  indicating a more symmetric light curve.

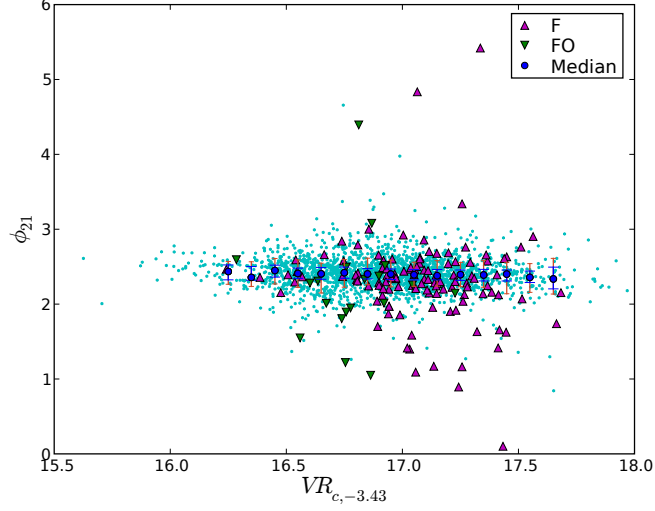


Fig. 12.—  $\phi_{21}$  against  $VR_c$  for all candidates. We find that  $\phi_{21}$  is similar for all candidates,  $r_{21}$  can be used as a measure of the ratio of the overall amplitud. Blue circles and error bars are as described in the caption of Figure 5. See caption of Figure 3 for description of remaining symbols.

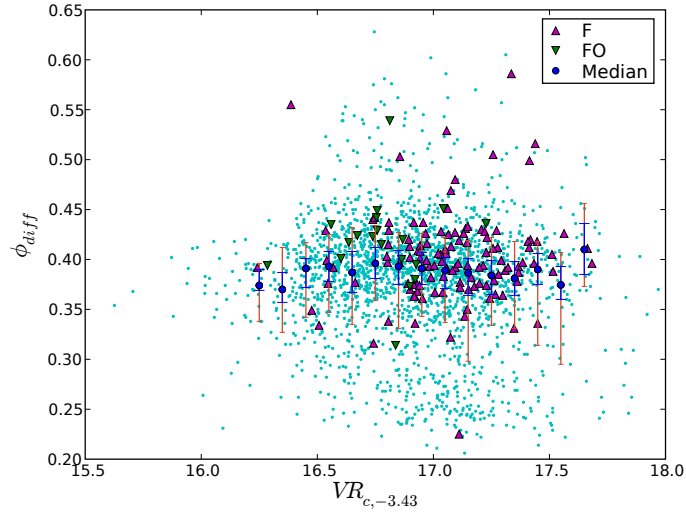


Fig. 13.—  $\phi_{diff}$  against  $VR_c$  for all candidates. Blue circles and error bars are as described in the caption of Figure 5. See caption of Figure 3 for description of remaining symbols. We find that the lag between  $\phi_{max}$  and  $\phi_{min}$  is similar for all candidates, though candidates pulsating in overtone modes tend to have  $\phi_{diff}$  greater than the median.  $\phi_{diff}$  closer to 0.5 indicates a more symmetric light curve.

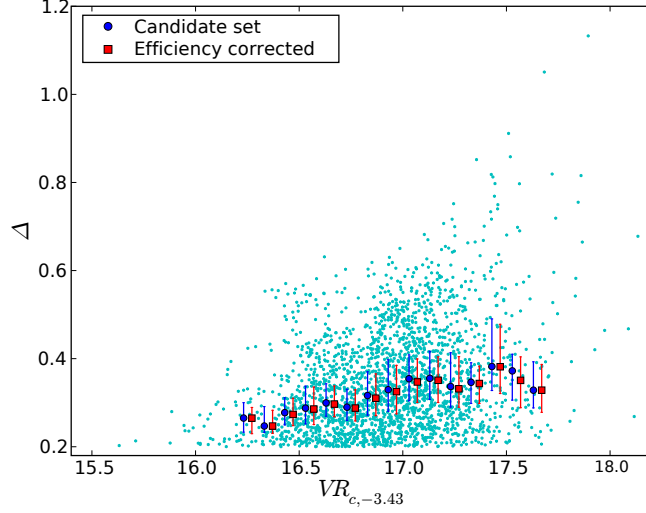


Fig. 14.— Efficiency corrected plot of amplitude against  $VR_c$ . We show a plot similar to Figure 10. The red squares show the efficiency-corrected median values. We show the original (blue circles) and corrected (red squares) 33<sup>rd</sup> percentile errors (see caption of Figure 5). For visibility, we show these values slightly offset from the center of the bin positions.

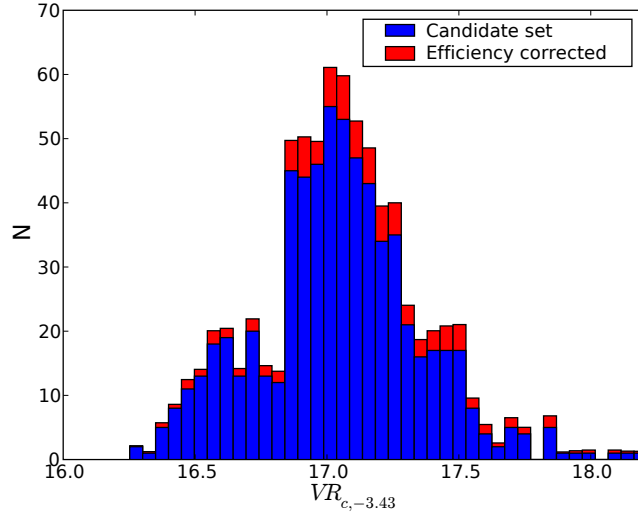


Fig. 15.— Efficiency corrected histogram of  $VR_c$  for only sources with  $\Delta > 0.4$ . The blue bars show the observed histogram, and the red bars give the efficiency-corrected histogram. We find an indication of an excess of larger amplitude, subluminal sources around  $VR_c = 17.4$ . This may be the subluminal population observed in Fornax by Poretti et al. (2008).

## REFERENCES

- Alard, C., & Lupton, R. H. 1998, *ApJ*, 503, 325
- Alard, C. 2000, *A&AS*, 144, 363
- Alcock, C., et al. 2000, *ApJ*, 536, 798 (a)
- Alcock, C., et al. 2000, *ApJ*, 542, 281 (b)
- Alcock, C., et al. 2000, *ApJ*, 542, 257 (c)
- Bono, G., Incerpi, R., & Marconi, M. 1996, *ApJ*, 467, L97
- Bono, G., Caputo, F., Cassisi, S., Castellani, V., Marconi, M., & Stellingwerf, R. F. 1997, *ApJ*, 477, 346
- Breger, M. 2000, *Delta Scuti and Related Stars*, 210, 3
- Cole, A. A., Tolstoy, E., Gallagher, J. S., III, & Smecker-Hane, T. A. 2005, *AJ*, 129, 1465
- Foster, G. 1995, *AJ*, 109, 1889
- Garg, A., et al. 2007, *AJ*, 133, 403
- Garg, A. 2008, Ph.D. Thesis, Harvard University (a)
- Garg, A. 2008, *American Institute of Physics Conference Series*, 1082, 263 (b)
- Harris, J., Zaritsky, D., & Thompson, I. 1997, *AJ*, 114, 1933
- Lepischak, D. S. 2007, Ph.D. Thesis, McMaster University
- McNamara, D. H. 2000, *PASP*, 112, 1096
- McNamara, D. H., Rose, M. B., Brown, P. J., Ketcheson, D. I., Maxwell, J. E., Smith, K. M., & Wooley, R. C. 2004, *IAU Colloq. 193: Variable Stars in the Local Group*, 310, 525
- McNamara, D. H., Clementini, G., & Marconi, M. 2007, *AJ*, 133, 2752
- Miknaitis, G., et al. 2007, *ApJ*, 666, 674
- Minniti, D., et al. 1998, *Fundamental Stellar Properties*, 189, 293
- Oestreich, M. O., Gochermann, J., & Schmidt-Kaler, T. 1995, *A&AS*, 112, 495
- Pigulski, A., Kołaczowski, Z., Ramza, T., & Narwid, A. 2006, *Memorie della Societa Astronomica Italiana*, 77, 223
- Poretti, E., et al. 2005, *A&A*, 440, 1097

- Poretti, E., et al. 2008, *ApJ*, 685, 947
- Poretti, E., et al. 2009, *A&A*, 506, 85
- Reegen, P. 2007, *A&A*, 467, 1353
- Reimann, J. D. 1994, Ph.D. Thesis
- Rest, A., et al. 2005, *ApJ*, 634, 1103
- Rest, A., & Garg, A. 2008, *American Institute of Physics Conference Series*, 1082, 294
- Schechter, P. L., Mateo, M., & Saha, A. 1993, *PASP*, 105, 1342
- Sebo, K. M., et al. 2002, *ApJS*, 142, 71
- Soszynski, I., et al. 2003, *Acta Astronomica*, 53, 93
- Soszynski, I., et al. 2008, *Communications in Asteroseismology*, 157, 41
- Soszyński, I. 2009, *IAU Symposium*, 256, 30
- Stellingwerf, R. F., Gautschy, A., & Dickens, R. J. 1987, *ApJ*, 313, L75
- Suárez, J. C., Garrido, R., & Goupil, M. J. 2006, *A&A*, 447, 649
- Wood-Vasey, W. M., et al. 2007, *ApJ*, 666, 694